

# SCIENTIFIC REPORTS



OPEN

## The Crotone Megalandslide, southern Italy: Architecture, timing and tectonic control

Massimo Zecchin<sup>1</sup>, Flavio Accaino<sup>1</sup>, Silvia Ceramicola<sup>1</sup>, Dario Civile<sup>1</sup>, Salvatore Critelli<sup>2</sup>, Cristina Da Lio<sup>3</sup>, Giacomo Mangano<sup>1</sup>, Giacomo Prosser<sup>4</sup>, Pietro Teatini<sup>3,5</sup> & Luigi Tosi<sup>3</sup>

Large-scale submarine gravitational land movements involving even more than 1,000 m thick sedimentary successions are known as megalandslides. We prove the existence of large-scale gravitational phenomena off the Crotone Basin, a forearc basin located on the Ionian side of Calabria (southern Italy), by seismic, morpho-bathymetric and well data. Our study reveals that the Crotone Megalandslide started moving between Late Zanclean and Early Piacenzian and was triggered by a contractional tectonic event leading to the basin inversion. Seaward gliding of the megalandslide continued until roughly Late Gelasian, and then resumed since Middle Pleistocene with a modest rate. Interestingly, the onshore part of the basin does not show a gravity-driven deformation comparable to that observed in the marine area, and this peculiar evidence allows some speculations on the origin of the megalandslide.

Kilometer- to tens of km-scale submarine gravitational collapses, here referred to as megalandslides, consist of land movements involving up to 1 km (or even more) thick sedimentary successions sliding on a basal surface that may classify as 'basal overpressured shale detachment' or 'salt detachment'<sup>1</sup>. Gravity gliding may be instantaneous, associated with mass wasting and shallow detachment, or slow, in connection with a deep detachment and long-term geological processes such as high sedimentation rates or uplift in adjacent areas<sup>1</sup>. These large-scale phenomena typically produce an updip extensional domain and a downdip contractional domain, which are linked via a basal detachment surface<sup>2,3</sup>. The interest for megalandslides has involved also the hydrocarbon industry, as they may be associated with structural traps consisting of large anticlines<sup>1</sup>.

Several examples were reported worldwide, mostly but not exclusively on passive margins, such as in the Bight Basin, Australia<sup>4</sup>, Niger Delta<sup>5–7</sup>, West African margins<sup>8–10</sup>, Gulf of Mexico<sup>11–13</sup>, Brazil<sup>14</sup>, Antarctic Peninsula<sup>15</sup>, and Brunei<sup>16</sup>. European examples (see Canals, *et al.*<sup>15</sup> and references therein) include the Storegga, Trænadjupet and Finneidfjord slides (Norwegian margin), BIG'95 Slide (off the Ebro river, Spain), Central Adriatic Deformation Belt (Adriatic margin, Italy), and Afen Slide (Faeroe-Shetland Channel).

The existence of a previously unknown, ca. 1,000 km<sup>2</sup> megalandslide in the Neogene Crotone Basin, southern Italy (Fig. 1A,B), was recently suggested by Minelli, *et al.*<sup>17</sup> on the basis of seismic, well and GPS data and literature information. The Crotone Basin is interpreted as a forearc basin located on the Ionian side of the Calabrian Arc (Southern Italy) (Fig. 1A); it is partly exposed in the Crotone area (Fig. 1B,C) and it is also widely documented offshore. The Calabrian Arc is interpreted as a composite terrane that migrated to the SE since the Middle Miocene in response to the subduction of the Ionian oceanic crust<sup>18–22</sup>. Migration was facilitated by the formation of major NW-trending shear zones, which are particularly frequent in the NE sector of the Calabrian arc and represent the NE and the SW boundaries of the Crotone Basin<sup>23–25</sup> (Fig. 1A,B). The sedimentary infill of the basin consists of Serravallian to Middle Pleistocene marine, coastal and continental deposits, which record main tectonic events and glacio-eustasy<sup>26–31</sup>. Since the Middle Pleistocene, the basin has undergone rapid uplift with an average rate of ca. 1 mm/yr<sup>32</sup>.

<sup>1</sup>(OGS) Istituto Nazionale di Oceanografia e di Geofisica Sperimentale, Borgo Grotta Gigante, 42/c, 34010, Sgonico, Trieste, Italy. <sup>2</sup>Dipartimento di Biologia, Ecologia e Scienze della Terra, Università della Calabria, 87036, Arcavacata di Rende, CS, Italy. <sup>3</sup>Institute of Marine Sciences, National Research Council, Arsenale - Tesa 104, Castello 2737/F, 30122, Venezia, Italy. <sup>4</sup>Dipartimento di Scienze, Università della Basilicata, Potenza, Italy. <sup>5</sup>Department of Civil, Environmental and Architectural Engineering, University of Padua, via Marzolo 9, 35121, Padova, PD, Italy. Correspondence and requests for materials should be addressed to M.Z. (email: [mzecchin@inogs.it](mailto:mzecchin@inogs.it)) or L.T. (email: [luigi.tosi@ismar.cnr.it](mailto:luigi.tosi@ismar.cnr.it))

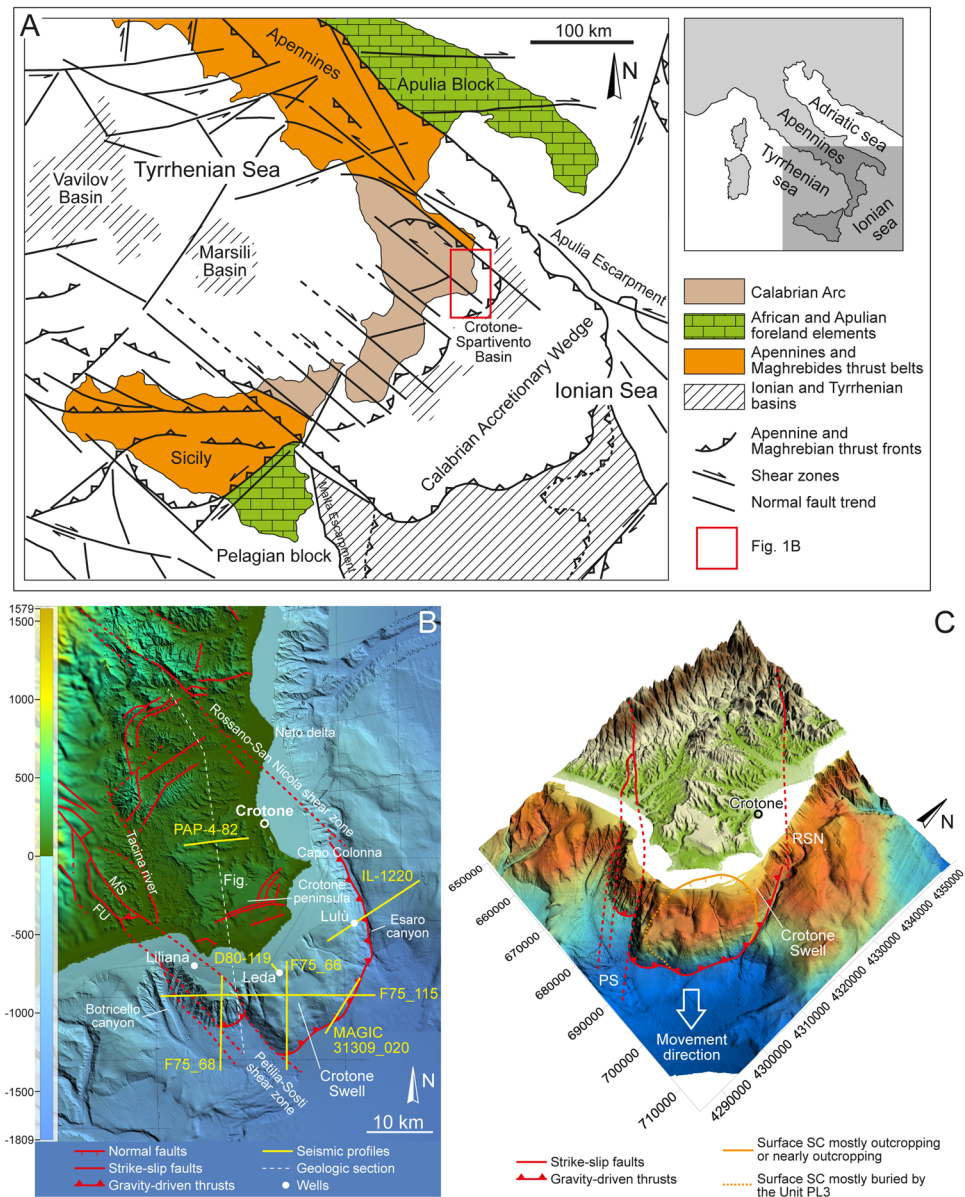


**Figure 1.** (A) Structural map of the Calabrian Arc, which is comprised between the southern Apennines and Sicily (modified from Van Dijk & Okkes<sup>24</sup>). The main structural elements and the Ionian and Tyrrhenian basins are highlighted. (B) DTM map showing the onshore and offshore parts of the Crotone Basin (see Fig. 1A for location). The selected seismic profiles and wells are shown. The illustrated faults are reported from various authors<sup>27,30,31,38</sup>. Abbreviations: FU and MS – Fosso Umbro and Marcedusa-Steccato faults. (C) Three-dimensional view of the Crotone basin highlighting the Crotone Swell, the extent of the recognized scar (surface SC, see text), and the thrust front showing SE-ward vergence (v. ex.  $7\times$ ). In (B) and (C), bathymetric data were acquired by OGS in the frame of the MaGIC (Marine Geohazards along the Italian Coasts) project; public DTM data are available from <https://www2.jpl.nasa.gov/srtm/>.

The interpretation of Minelli, *et al.*<sup>17</sup> indicates that most part of the Messinian to Plio-Pleistocene succession of the Crotone Basin (both onshore and offshore) is gliding toward the Ionian Sea above a Messinian halite layer. Evidence of large-scale gravity tectonics affecting Pliocene strata was already reported in previous studies<sup>33</sup>. The megalandslide would be characterized by a downdip contractional domain located offshore and corresponding to the prominent Crotone Swell (Fig. 1B,C), and an onshore updip domain, represented by some seaward-dipping normal faults found in the northern part of the basin<sup>17</sup> (Fig. 1B).

However, many uncertainties remain about the origin, timing, extent and existence itself of the large-scale gravitational phenomenon involving the Crotone Basin. This generalized uncertainty is highlighted by the different interpretation provided by other authors about the nature of the Crotone Swell<sup>34</sup>, and by the modest deformation and overall good preservation of the Messinian to Plio-Pleistocene succession in the onshore part of the basin, which even contains stratotypes<sup>27,28</sup>. Much more evidence is therefore necessary to address this question.

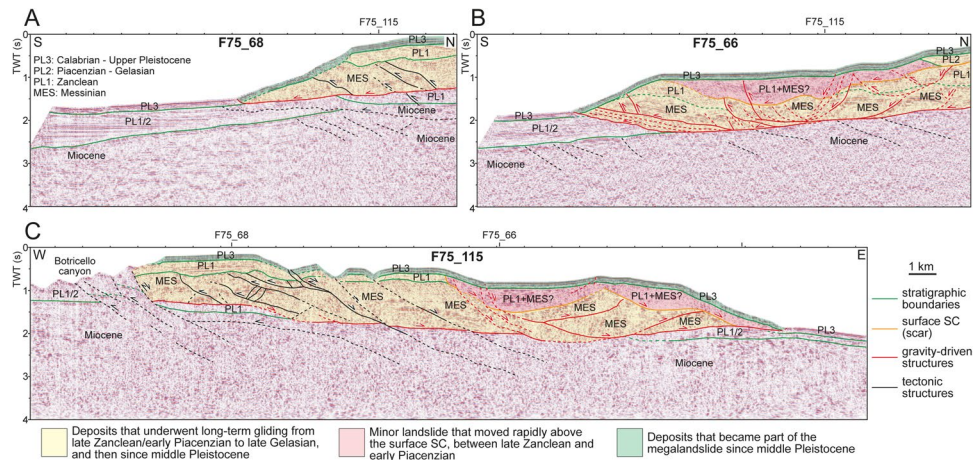


**Figure 2.** (A,B,C) Interpreted seismic profiles that cross-cut the Crotona Swell (Fig. 1B for location), interpreted to as a megalandslide. SW-verging tectonic structures (in black) are truncated by SE-verging, inferred gravity-driven structures (in red), which are dominated by a basal detachment surface and a thrust front that reaches the seafloor. The gravity-driven phenomenon involves Late Miocene and Plio-Pleistocene deposits, which in seismic profiles correspond to seismic units (Units MES and PL1-3) separated by unconformities. The ages of the seismic units are derived from the available wells (Fig. 5). A minor landslide of inferred mid-Pliocene age is nested in the megalandslide and is bounded at the base by a scar (surface SC). The timing of the gravity-driven process (see areas with different color) is discussed in the text. Seismic data from “Visibility of Petroleum Exploration Data in Italy” (ViDEPI Project) (<http://unmig.sviluppoeconomico.gov.it/videpi/>). Uninterpreted seismic profiles are available in Supplementary Material Fig. S1.

Moreover, the existence of a still active large-scale gravitational collapse involving the onshore part of the basin would have social impacts, as it would raise security concerns about the population of this area, where the city of Crotona (64.000 inhabitants) is located.

The present study is aimed at resolving the existence, areal extent and timing of the Crotona Megalandslide. This has been achieved by integrating on- and offshore datasets acquired across the Crotona Swell and in the onshore part of the basin, including seismic, morpho-bathymetric, sediment cores, outcrops and land movements.

## Results

**The offshore area.** South of the Crotona peninsula, the Crotona Swell, a morphological high 16 km long and 30 km wide, is characterized by a prominent lobate morphology with an undulated longitudinal profile (Fig. 1B,C). The high includes a portion of continental shelf from 5 to 10 km wide. The continental slope is subdivided in an upper slope characterized by a flat, NE-SW elongated intraslope basin (at ca. 600 m water depth), and a rather steep (up to 11°) lower slope from 750 m to 1350 m water depth, which is incised by several single and multiple scars up to 5 km wide showing ‘fresh’ morphologies. The Crotona Swell is bounded by two well incised and elongated canyon systems: the Botricello, a quite short (40 km) NW-trending system and the Esaro, a NS-trending asymmetric system developing along the eastern side of the morphological high (Fig. 1B,C).

The Crotona Swell exhibits a complicated structure, consisting of an offshore (SE-ward) verging thrust, locally passing updip, via a seaward-dipping detachment surface inclined ca. 3° to 4°, into SE-ward-dipping extensional faults (Figs 1B,C, 2 and 3A). Orientation of tectonic structures can be easily ascertained by correlating them in differently oriented seismic lines (Fig. 2). The main contractional structure intersects the seafloor at the base of the slope (Figs 1C, 2, 3A and 4), whereas the basal detachment surface truncates older NE-dipping and SW-verging thrusts (Fig. 2). Minor contractional and extensional structures involve the main body, which is up to 1.5 s TWT (ca. 1.6 km) thick and extends for an area of ca. 25 × 15 km (Figs 1B,C and 2). Based on the available wells, the sedimentary succession that composes the Crotona Swell above the basal detachment surface consists of evaporites and clastic sediments of Messinian age, and of Plio-Pleistocene deep-marine deposits (Fig. 5). Near the thrust front, the basal detachment surface places this succession above either Miocene or Plio-Pleistocene deposits, depending on the trajectory of the thrust surface or on the overall geometry of the footwall strata (Figs 2 and 3A). The amount of shortening produced by thrusting cannot be ascertained with precision, but it is in the order of several kilometers (at least 10 km based on the F75\_68 seismic profile; Figs 1B and 2A), whereas a minor amount of extension, in the order of some hundreds of meters, is associated with the recognized normal faults (Fig. 2B).

In W-E trending transects (Fig. 2C), the SE-ward directed thrust sheet seems to interfere with NW-trending, NE-dipping faults that are inferred to be part of the major Petilia-Sosti regional shear zone<sup>24</sup> (Fig. 1B), which was characterized by alternating sinistral and dextral transpressional and transtensional activity during the Plio-Pleistocene times<sup>31</sup>. In particular, two main branches of the Petilia-Sosti shear zone are recognizable in the F75\_115 seismic profile (Fig. 2C); they likely represent the seaward extension of the Marcedusa-Steccato and Fosso Umbro faults identified onshore (Fig. 1B). The late middle Pleistocene activity of these faults has been interpreted as related to their reactivation as dextral transfer faults during formation of local extensional and

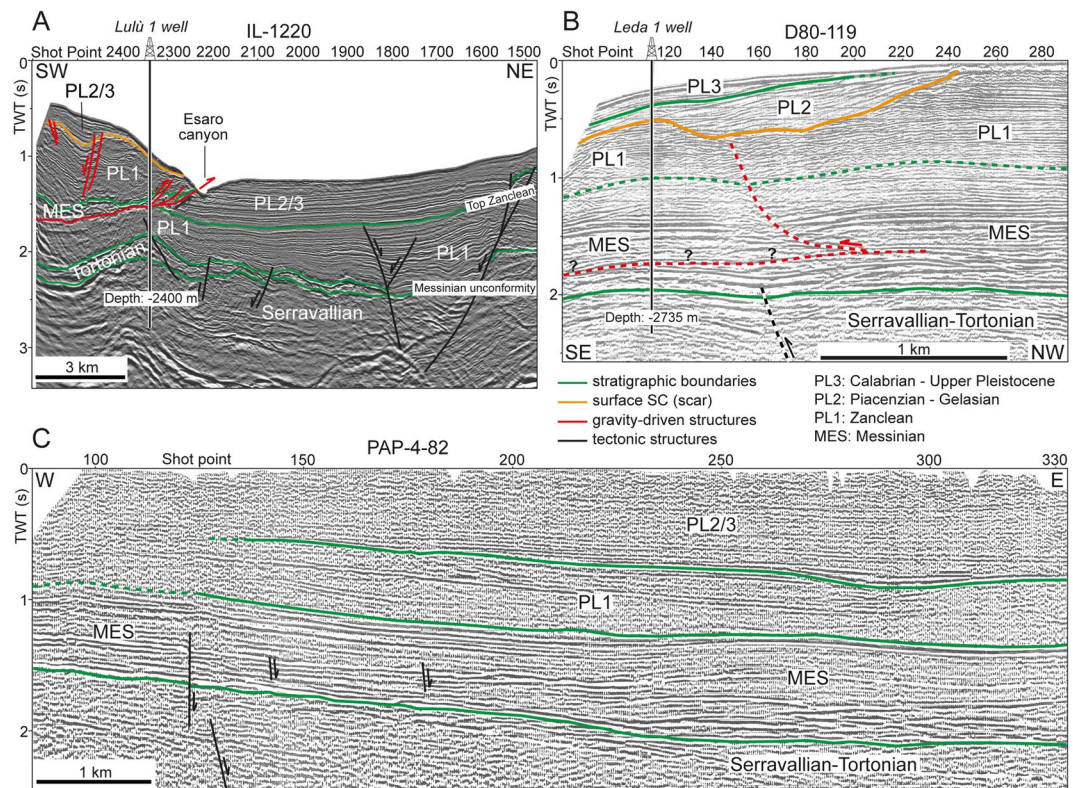


**Figure 3.** (A) The IL-1220 seismic profile, which cross-cut the eastern margin of the Crotona Swell (modified from Zecchin, *et al.*<sup>30</sup>, Fig. 1B for location). Note that the thrust front seems to reach the western wall of the Esaro canyon. The stratigraphy of the Lulù 1 well is shown in Fig. 5. (B) The D80-119 seismic profile, which is close to the northern part of the F75\_66 seismic profile (modified from Zecchin, *et al.*<sup>30</sup>, Fig. 1B for location). Note the proximal part of the scar (surface SC) that truncates the Zanclean deposits (Unit PL1) and is in turn overlain by undisturbed Piacenzian and Gelasian deposits (Unit PL2). Note also the uncertain detection of the basal detachment surface, which is visible just to the south (see Fig. 2B). The stratigraphy of the Leda 1 well is shown in Fig. 5. (C) The PAP-4-82 seismic profile, which is located onshore (modified from Zecchin, *et al.*<sup>27</sup>, Fig. 1B for location). Note the nearly undisturbed sedimentary succession that characterizes the central part of the Crotona Basin. Seismic data from “Visibility of Petroleum Exploration Data in Italy” (ViDEPI Project) (<http://unmig.sviluppoeconomico.gov.it/videpi/>).

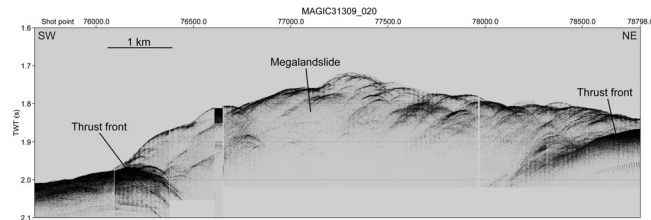


**Figure 4.** Subbottom profile cross-cutting the front of the megalandslide (Fig. 1B for location). Note that the basal thrust front reaches the seafloor, suggesting modern or recent activity. The profile has been acquired during the MaGIC (Marine Geohazards along the Italian Coasts) geophysical campaign onboard of the R/V OGS Explora in April 2009.

contractional gravity-driven structures, connected to SE-directed seaward gliding of part of the sedimentary infill of the Crotona Basin<sup>31</sup>. Following this interpretation, it is inferred that reactivation of the NW-trending structures drove the SE-ward movement of the whole Crotona Swell toward the Ionian Sea (Fig. 1B,C). This observation allows discriminating the structures related to the SE-ward movement of the Crotona Swell from older contractional structures, which show a SW-ward vergence and either are sealed by a surface representing the top of the Messinian succession or were active during Pliocene time (Fig. 2). It is also to be noted that just east of the Petilia-Sosti shear zone, the thrust front is shifted of ca. 8 km to the SE with respect to the thrust segment that is comprised between the seaward parts of the Marcedusa-Steccato and Fosso Umbro faults, where the F75\_68 seismic profile has been acquired (Fig. 1B,C).

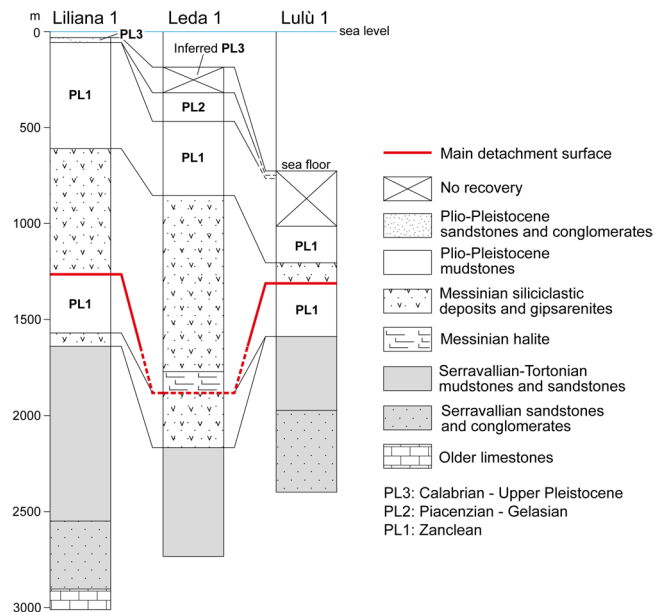


**Figure 5.** Simplified stratigraphy of the three wells considered in this study (Fig. 1B for location). PL1-3 correspond to the seismic units recognized in the seismic profiles (Figs 2 and 3). Data from “Visibility of Petroleum Exploration Data in Italy” (ViDEPI Project) (<http://unmig.sviluppoeconomico.gov.it/videpi/>).

Seismic profiles document that an irregular, composite surface (surface SC), sealed by undeformed Piacenzian to Gelasian deposits (Unit PL2), truncates the Zanclean succession (Unit PL1) landward with respect to the main thrust front and tends to approach the seafloor toward the shoreline and along the eastern slope of the Crotona Swell (Figs 1C, 2B,C and 3A,B). This irregular surface may be followed downdip in the SE part of the Crotona Swell, where it truncates also Messinian deposits and is overlain by a deformed landmass up to 0.7 s TWT (ca. 0.7 km) thick (F75\_66 and F75\_115 seismic profiles; Fig. 2B,C). The F75\_66 seismic profile documents that the reflectors of the undeformed Unit PL2 onlaps or downlaps the landward part of the deformed landmass (Fig. 2B). These observations are consistent with the presence of deposits not younger than Zanclean (Units PL1 and MES) within the deformed landmass (Figs 2B,C and 3A,B). The landmass was in turn dissected by both extensional and contractional structures (Fig. 2B) that possibly propagated from reactivation of pre-existing faults in the deeper part of the Crotona Swell and/or by newly formed structures that crosscut the whole succession.

All the described features are sealed by a sedimentary drape up to 0.15 s TWT (ca. 150 m) thick of inferred Calabrian to late Pleistocene age (Unit PL3; Figs 2 and 3B), which, excepting for the main thrust at the base of the modern slope, at the seismic scale is affected by only minor faults with negligible offset, probably produced by relatively recent reactivation of older faults. The surface bounding the base of the Unit PL3 is associated with a hiatus that increases seaward. This encompasses the whole Pliocene and Early Pleistocene (Gelasian) in the lower part of the modern slope (Fig. 2B). At the base of the modern slope, the Unit PL3 is affected by a thrust that produces a shortening not greater than 500 m (Fig. 2). Along the relatively steep portion of the slope, the Unit PL3 exhibits local irregular reflections, possibly due to gravitational collapses (Figs 2A and 4).

**The onshore area.** In the onshore sector of the Crotona Basin, Serravallian to Middle Pleistocene continental to deep-marine deposits lie in an area that extends for ca. 45 × 30 km (Fig. 1B). SSE- and SE-ward dipping normal faults found in the Crotona peninsula and in the northern part of the Crotona Basin (Fig. 1B), show vertical displacements ranging from m- to hm-scale and lengths up to 10 km<sup>27,35</sup>. Part of these faults are thought to have been originated by gravity-driven processes during both Pliocene and Pleistocene times<sup>27,31</sup>. Salt diapirs and related tectonic structures were also recognized in the northern part of the basin<sup>27,36</sup>. However, seismic profiles (Fig. 3C) and field observations in the onshore portion of the basin do not document the presence of a mega-detachment involving the Messinian to Pleistocene succession such as to justify the km- to tens of km-scale displacement visible offshore.

The measurements of land movements available from permanent GPS stations and SAR-based interferometry also highlight a complex picture of the ground dynamics of the area (Fig. 6). The average magnitude and direction of the horizontal displacements provided by each GPS stations over the last decade are shown in Fig. 6A. SAR interferometry provides a much more detailed picture of the displacements, even if only in the west-east direction (Fig. 6B) because of the satellite movement along a polar (i.e., north-south) orbit. The west-east displacement map, which has been obtained by properly combining Cosmo-SkyMED images acquired over the 2011–2014 period in ascending and descending mode, reveals that the horizontal movements are characterized by a very complex pattern with uneven values. In particular, significant eastward movements (up to 4–5 mm/yr) are detected only between the Neto river delta and Capo Colonna, and in part of the Tacina river valley to the west (Fig. 6B). Patched positive (i.e., eastward) and negative (i.e. westward) displacements are measured

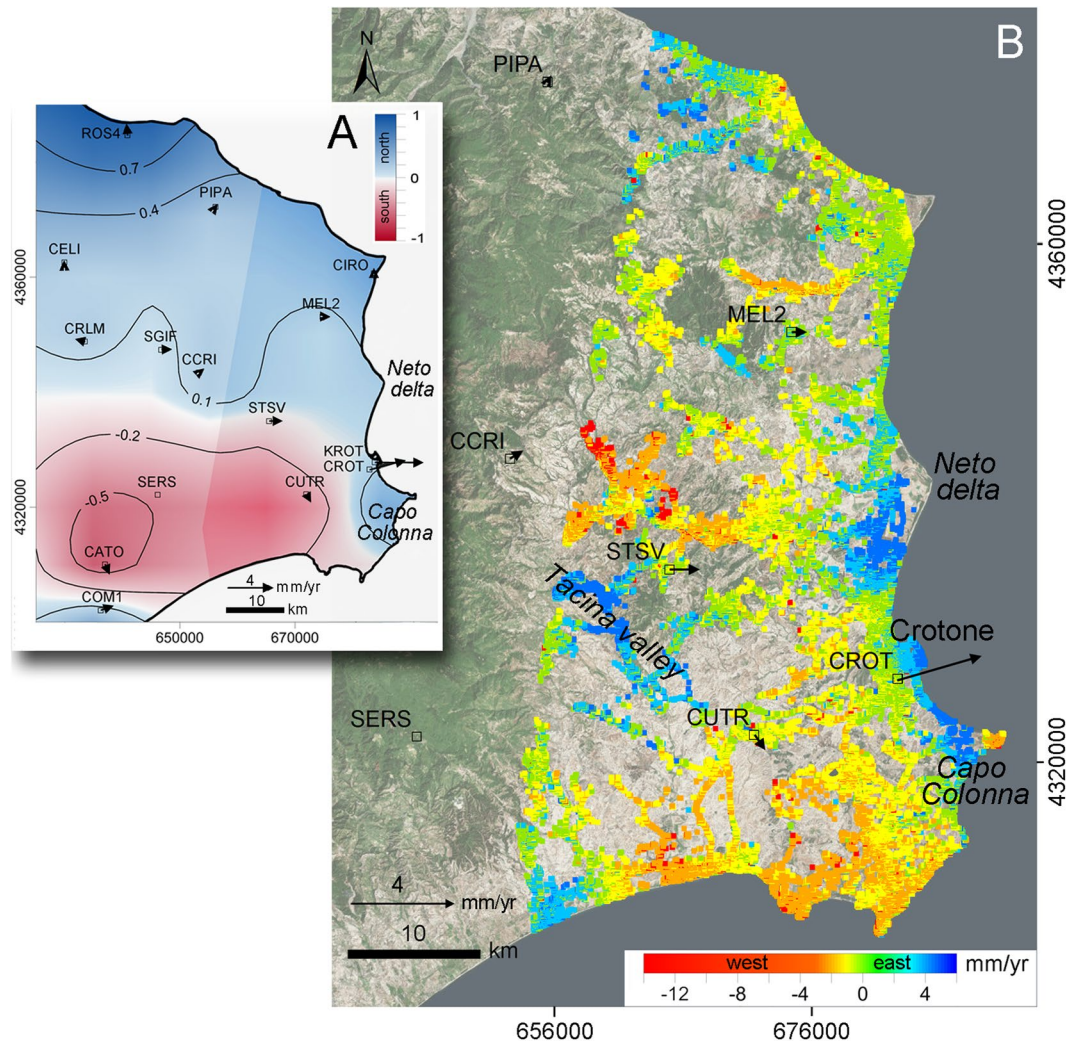


**Figure 6.** Maps of the ground movements. (A) GPS velocities superposed to the interpolated map of south-north displacements referred to SERS. (B) Average west-east ground movements obtained by SAR-based interferometry over the 2011–2014 period. Black squares show the positions of the GPS stations, with the arrows providing the direction and magnitude of the horizontal displacement rate. Satellite base map used is from Esri, DigitalGlobe, GeoEye, Earthstar Geographics, CNES/Airbus DS, USDA, USGS, AeroGRID, IGN, and the GIS User Community.

elsewhere, with relatively small values (in general less than 1–2 mm/yr). Interpolation of the south-north component obtained by GPS data partly overcomes the SAR mapping restriction (Fig. 6A) and shows a regional trend with values smaller than 1 mm/yr. In the northern and central parts of the basin the rates are even smaller.

Therefore, the updip termination of the sedimentary body that underwent seaward migration remains obscure, with both GPS and SAR data highlighting that the Messinian to Pleistocene succession does not glide radially toward the Ionian Sea, as proposed in previous studies<sup>17</sup>.

## Discussion

The present study proves that the Crotona Swell is a tens of km-scale megalandslide up to 1.5 s TWT (ca. 1.6 km) thick subjected to gravity gliding processes<sup>1</sup>. This is revealed by the presence of a basal detachment surface dipping seaward of 3–4°, which connects an extensional updip domain, consisting of seaward-dipping normal faults, with a compressional downdip domain (Figs 2 and 3A,B). Such an interpretation contrasts with previous ones that described the Crotona Swell as the result of a SW-verging tectonic-driven thrust<sup>27,34</sup>.

A novelty of the present study is the discovery of a gravitational collapse nested in the main gravitational body and involving Messinian and Zanclean deposits (Units MES and PL1) (Figs 1C, 2B,C and 3A,B). This collapse is marked by a composite scar (surface SC) that is sealed by undisturbed Piacenzian-Gelasian deposits (Unit PL2) in its updip sector and tends to approach the seafloor landward (Figs 1C, 2B,C and 3A,B). This observation, together with the evidence that almost all structures are draped by Quaternary sediments (Unit PL3; Figs 2 and 3A,B), suggests that the seaward movement of the whole megalandslide started between Late Zanclean and Early Piacenzian times and continued until roughly Late Gelasian (Figs 2 and 7A–D), as demonstrated by local

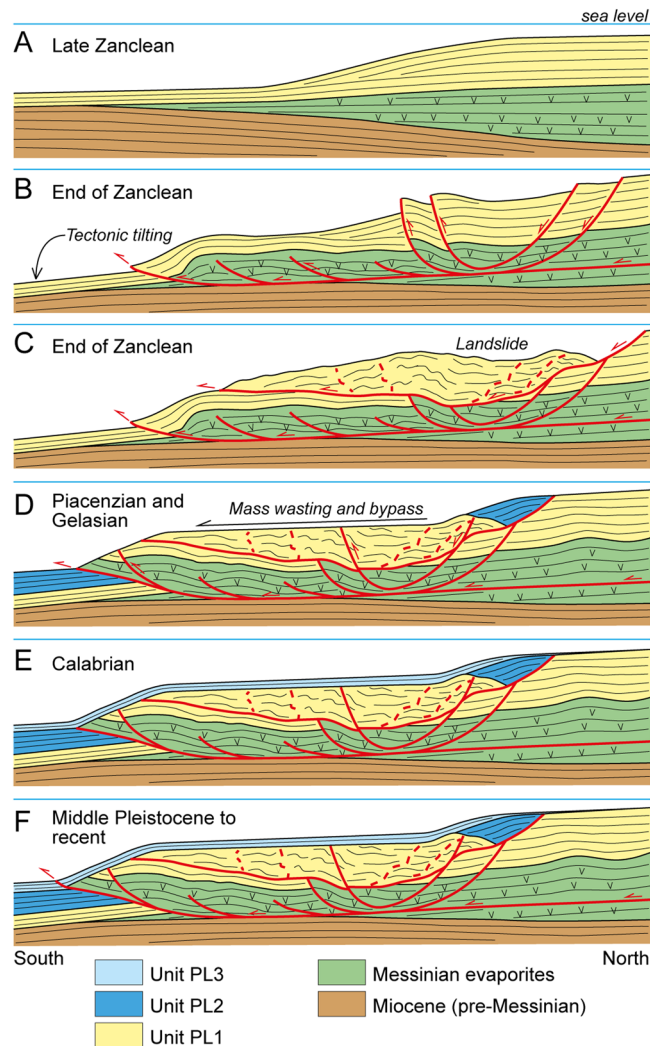


**Figure 7.** Inferred evolution of the seaward part of the Crotono megalandslide (not to scale), inspired by the F75\_66 seismic profile (Fig. 2B). After a relatively tranquil phase of shelf margin progradation during Zanclean time (A), a tectonic event between Late Zanclean and Early Piacenzian (see text) led to tilting and triggered the gravity-driven movement (B). A minor landslide formed on top of the already moving megalandslide, leading to an exposed scar landward (C). Piacenzian to Gelasian deposits accumulate above the scar and the proximal part of the minor landslide, as well as in the deep basin, during a long-term phase of relatively slow movement of the megalandslide (D). A continuous sediment drape accumulated during an inferred phase of paucity of movement during Calabrian time (E). Since middle Pleistocene, the movement of the megalandslide has reactivated with modest rate, and still continues today (F).

minor gravity-related faults affecting the surface SC and the deformed landmass in the seaward sector (Fig. 2B). Moreover, since the formation of the surface SC postdated the Unit PL1 and predated the Unit PL2 (Figs 2B, 3B and 7C,D), the gravitational collapse locally involving the upper part of the megalandslide, and in general the onset of the large-scale movement of the latter, were probably rapid. In contrast, the large hiatus associated with the surface bounding the base of the Unit PL3 in slope settings, suggests that the whole megalandslide continued to glide relatively slowly above the basal detachment surface until Late Gelasian (Figs 2 and 7D). This produced the observed km-scale seaward dislocation associated with the main gravity-driven thrust and prevented the accumulation of the Unit PL2 due to substrate instability, implying also that the accumulation of the Unit PL2 in basinal settings was contemporaneous to the progressive seaward gliding of the whole landmass (Fig. 7D). Once the movement of the megalandslide ceased, the Calabrian to late Pleistocene Unit PL3 started to accumulate and later was in turn affected by a reactivation of the gravitational phenomenon (Figs 2 and 7E,F). The hm-scale dislocation of the Unit PL3 by the main thrust at the base of the slope points to a very modest post-Gelasian activity, although the involvement of the seafloor suggests that it is still active (Figs 3A and 4).

The inferred Late Zanclean-Early Piacenzian age for the onset of the activity of the megalandslide (Fig. 7B,C) strongly suggests that a well-known mid-Pliocene (ca. 3.7 Ma) compressional-transpressional tectonic event, which affected the whole Calabrian Arc and produced thrusting and basin inversions<sup>23,27,30,37</sup>, was the triggering mechanism. In contrast, the end of the main seaward gliding of the megalandslide during Gelasian time

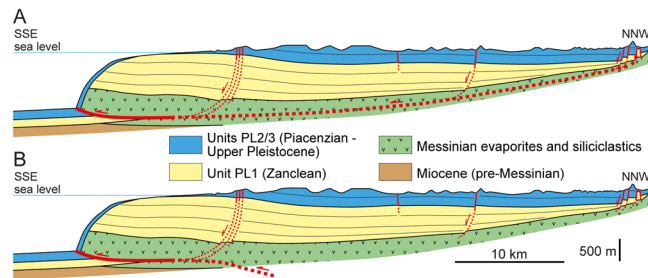


**Figure 8.** Simplified onshore-offshore geologic section (Fig. 1B for location) reporting two contrasting models to explain the development of the Crotona megalandslide. For a better reading, the recognized seismic units (Figs 2 and 3) are shown. (A) In the hypothesis that the gravity-driven movement involves the whole Crotona Basin, the basal detachment surface would connect the frontal thrust with seaward-dipping normal faults found to the north. Note that the dislocations associated with the normal faults are unable to justify the km-scale displacement associated with the frontal thrust. (B) Alternatively, the frontal thrust might have initiated as tectonic thrust during the mid-Pliocene tectonic event (see text) and be rooted at depth via a NW-ward dipping ramp in more landward position. In this case, only the offshore part of the sedimentary succession, corresponding to the Crotona Swell, would have been reactivated as gravitational collapse, and no detachment surface would be present in most of the onshore part of the basin fill.

(Fig. 7D,E) is roughly coincident with an episode of increased tectonic subsidence and basin collapse started at ca. 2.2 Ma, which involved the currently exposed part of the Crotona Basin and is reflected by the opening of the Marsili Basin in the Tyrrhenian Sea<sup>27,30</sup>. This tectonic episode may have led to deepening and to a decrease of the local slope toward the Ionian Sea, which halted the seaward gliding of the megalandslide. The Quaternary reactivation of the gravitational phenomenon, affecting also the Unit PL3 (Fig. 7F), was possibly triggered by the regional uplift involving the Crotona Basin since Middle Pleistocene (starting from ca. 0.45 Ma<sup>27</sup>), which reached maximum rates just south of the Crotona city<sup>32</sup> and may have increased the dip of the seafloor toward the Ionian Sea. Alternatively, the reactivation might have been triggered by another known compressional-transpressional tectonic event occurred at ca. 1.1 Ma<sup>27,30,31</sup>. However, since the gravitational phenomenon seems to be still active, as demonstrated by the seafloor disturbance of the main thrust (Figs 3A and 4), a more recent reactivation of the megalandslide associated with the regional uplift is favored. Moreover, the concomitant relative sea-level drops associated with the Late Quaternary, high-magnitude glacio-eustatic changes may have favored the gravitational movement.

In contrast to what was postulated by Minelli, *et al.*<sup>17</sup>, who assume a radial gliding toward the Ionian Sea, present data indicate that the gravity-driven structures have SE-ward vergence (Fig. 2), which was controlled by the reactivation with dextral shear sense of the NW-trending Petilia-Sosti shear zone, thus representing the southwestern boundary of the megalandslide (Fig. 1B,C). At present, a similar role of transfer fault with respect to the megalandslide is not documented for the shear zone that represents the northern boundary of the Crotona Basin (i.e., the Rossano-San Nicola shear zone, Fig. 1B,C). The non-homogeneous eastward movements spanning from less than 0.5 to about 5 mm/yr provided by interferometric SAR-data, together with the negligible N-S velocity field obtained by GPS data (Fig. 6A,B), suggest that active structures and/or local gravitational phenomena involve the onshore sector, further denying a radial gliding of the structure.

The evidence discussed above allows us to estimate the rate of the seaward movement of the megalandslide. Assuming a minimum shortening associated with the thrust front of 10 km (based on the F75\_68 seismic profile), and that the long-term gliding initiated at 3.7 Ma and terminated at 2.2 Ma, a minimum displacement rate of 6.7 mm/yr to the SE is expected during this phase. However, the displacement rate of the megalandslide may have been even locally greater, in particular if the observed additional shift of ca. 8 km to the SE of the thrust front just east of the Petilia-Sosti shear zone (i.e., east of the F75\_68 seismic profile; Fig. 1B) is mainly related to differential gravity-driven gliding rather than regional strike-slip tectonics. In contrast, assuming that the Quaternary reactivation of the gravitational phenomenon started at ca. 0.45 Ma, at the onset of the regional uplift, and taking into account that the maximum offset of the Unit PL3 is ca. 500 m (Fig. 2), a significantly more modest displacement rate of ca. 1 mm/yr would be associated with the most recent gliding phase.

A peculiar aspect is represented by the landward prosecution of the main detachment surface at the base of the megalandslide, and therefore the scale of the seaward-moving landmass. Assuming that the detachment surface led to the seaward gliding of the whole onshore part of the Messinian to Plio-Pleistocene deposits of the Crotona Basin (Fig. 8A), as advocated previously<sup>17</sup>, it is remarkable that this sedimentary succession remained nearly undeformed (Fig. 3C), excepting for some m- to hm-scale high-angle normal faults found in the northern part of the basin and in the Crotona peninsula (Fig. 1B). This situation would be very unusual, as the body of giant slides is commonly rather deformed<sup>15,16</sup>. The onshore part of the detachment surface would lie near the base of the Messinian strata (Fig. 8A), probably at the halite layer, and would be parallel to the bedding and impossible to discriminate from stratal surfaces in seismic profiles (Fig. 3B,C). The evidence of salt diapirism in the northern part of the basin might be associated with extension of the updip domain and to a local mobile layer. However, the non-homogeneous GPS and SAR data (Fig. 6) suggest that at least at present, an overall SE-ward migration of the onshore part of the basin fill does not occur. Moreover, the lacking evidence of chaotic structures linked to a



mega-detachment zone in the hypothetical onshore updip domain (Fig. 8A), which could justify the horizontal displacement observed offshore, makes the situation even more unusual and allows some speculations.

A first possibility is that the Messinian to Zanclean part of the succession shifted to the SE of several km, aided by the halite layer and driven by the two NW-trending shear zones, just since the mid-Pliocene tectonic event, leaving behind an area deprived of such a succession. In fact, in the Cirò area, north of Crotona, the Piacenzian succession directly lies on Tortonian deposits without interposed Messinian and Zanclean deposits<sup>38</sup>, but such a situation is not recognizable along the NW margin of the basin. Following a second alternative hypothesis, most of the shortening associated with the main offshore thrust might be related to compressional tectonics during the mid-Pliocene tectonic event, and then such a structure might have been reactivated later as gravitational collapse only in the offshore sector (Fig. 8B). In this latter hypothesis, the mid-Pliocene thrust would be rooted at depth via a NW-ward dipping ramp in more landward position, and no detachment surface in the Messinian succession would be present in most of the onshore part of the basin fill (Fig. 8B). Only the seaward-dipping faults found in the Crotona peninsula would be linked to the detachment surface (Fig. 8B). The availability of more subsurface data would confirm one of the two hypotheses presented above as well as provide a new interpretation.

Finally, although still active, the Quaternary seaward migration of the subaqueous part of the megalandslide, in the order of only few hundreds of meters in the last 0.5 Ma, seems to be very modest if compared to its Pliocene counterpart, and therefore it is expected not to significantly affect human activities in the onshore sector of the basin. However, recent gravity-driven phenomena along the modern Calabrian slope may represent the testimony of the modern, low-rate seaward migration of the large-scale landmass, an aspect to consider for any offshore activity.

## Methods

2D multichannel seismic profiles and well logs used in this study (Figs 2, 3 and 5) have been made available by the Ministry of the Economic Development in the framework of the project “Visibility of Petroleum Exploration Data in Italy” (ViDEPI) (<http://unmig.sviluppoeconomico.gov.it/videpi/>).

Concerning the F75\_66, F75\_68 and F75\_115 seismic profiles (Fig. 2 and Supplementary Material Fig. S1), the seismic images were converted into SEG-Y files by using a home-made code that includes parts of Seismic Unix software<sup>39</sup>. A Kirchhoff post-stack time migration was then applied to the data by using information about the velocities obtained for application of the normal move out labelled in the original figure. In order to obtain a better seismic image and avoiding artifacts such as smiles, the velocity fields were decreased of 20%. A band pass filtering was then applied to remove the random noise produced by migration.

Bathymetric data (Fig. 1B,C) and the OGS subbottom profile MAGIC31309\_020 (Fig. 4) were acquired by OGS in the frame of the MaGIC (Marine Geohazards along the Italian Coasts) project. The subbottom profile was acquired during a geophysical campaign onboard of the R/V OGS Explora in April 2009 using CHIRP II Benthos CAP-6600 system, comprising 16 hullmounted transducers operating at frequencies of 2–7 kHz (submetric vertical resolution).

All spatial data were gathered in a digital GIS. Seismic facies and horizons were identified on seismic reflection profiles and correlated to stratigraphic data available from wells. The conversion from time to depth in seismic profiles was done by comparing seismic data with closer wells and by using average time-depth relationships based on available interval velocities. On these basis, main seismic units, stratigraphic surfaces and faults were defined and their significance was interpreted.

Land movements are based on the Persistent Scatterer Interferometry (PSI) products made available by the Italian Ministry of the Environment and Protection of Land and Sea (<http://www.pcn.minambiente.it>). Specifically, we used COSMO-SkyMed frames 60, 62, 63, 64, consisting of a stack of 45 and 40 stripmap images acquired between 2011 and 2014 in ascending and descending mode, respectively. For the specific PSI processing, refer to Costantini, *et al.*<sup>40</sup>

The interferometric products (Fig. 6B) have been calibrated and de-flattened by the use of correction planes<sup>41,42</sup>, modeled through the velocities time series data recorded by PIPA, MEL2, CCRI, CROT, CUTR, STSV and SERS permanent GPS stations available from MAGNET GPS network (<http://geodesy.unr.edu>). Firstly, SERS (Fig. 6B), which is located outside the most part of the Crotona megalandslide, was selected to setup a local reference frame<sup>43</sup>. Secondly, the GPS velocities were projected along the Line-of-Sight (LOS) direction for each interferometric product. Finally, the average vertical ( $u_z$ ) and east-west ( $u_x$ ) ground movements (Fig. 6B) referred to SERS were computed by solving the linear system of equations (1):

$$\begin{cases} u_{asc} = u_x n_{x,asc} + u_z n_{z,asc} \\ u_{desc} = u_x n_{x,desc} + u_z n_{z,desc} \end{cases} \quad (1)$$

where  $u_{asc}$  and  $u_{desc}$  are the components of the displacement vector  $\mathbf{u}$  along the LOS ascending and descending direction;  $n_{x,asc}$ ,  $n_{z,asc}$ ,  $n_{x,desc}$ ,  $n_{z,desc}$  are the direction cosines identifying the satellite LOS vector for ascending and descending acquisition, respectively. Because of the different localization of reflecting Point Targets (PTs) in the two modes, the  $\mathbf{u}$  has been resampled on a regular cell-grid of  $50 \times 50 \text{ m}^2$  averaging the movement of the PTs belonging to the same cell<sup>44,45</sup>.

## References

- Morley, C. K., King, R., Hillis, R., Tingay, M. & Backe, G. Deepwater fold and thrust belt classification, tectonics, structure and hydrocarbon prospectivity: a review. *Earth-Sci Rev* **104**, 41–91, <https://doi.org/10.1016/j.earscirev.2010.09.010> (2011).
- Brun, J.-P. & Fort, X. Compressional salt tectonics (Angolan margin). *Tectonophysics* **382**, 129–150 (2004).
- Vendeville, B. C. Salt tectonics driven by sediment progradation: Part I - Mechanics and kinematics. *AAPG Bull* **89**, 1071–1079 (2005).

4. Totterdell, J. M. & Krassay, A. A. The role of shale deformation and growth faulting in the Late Cretaceous evolution of the Bight Basin, offshore southern Australia. In: *Subsurface Sediment Mobilization* (Eds Van Rensbergen, P., Hillis, R.R., Maltman, A.J. & Morley, C.K.), Geological Society (London) Special Publication **216**, 429–442 (2003).
5. Morley, C. K. & Guerin, G. Comparison of gravity-driven deformation styles and behaviour associated with mobile shales and salt. *Tectonics* **15**, 1154–1170 (1996).
6. Ajakaiye, D. E. & Bally, A. W. Manual and atlas of structural styles. *Niger Delta: AAPG Continuing Education Course Notes Series* **41**, 1–102 (2002).
7. Cobbold, P. R., Clarke, B. J. & Loseth, H. Structural consequences of fluid overpressure and seepage forces in the outer thrust belt of the Niger Delta. *Pet Geosci* **15**, 3–15 (2009).
8. Hudec, M. R. & Jackson, M. P. A. Regional restoration across the Kwanza Basin, Angola: salt tectonics triggered by repeated uplift of a metastable passive margin. *AAPG Bull* **88**, 971–990 (2004).
9. Jackson, M. P. A., Hudec, M. R., Jennette, D. C. & Kilby, R. E. Evolution of the Cretaceous Astrid thrust belt in the ultradeep-water Lower Congo Basin, Gabon. *AAPG Bull* **92**, 487–511 (2008).
10. De Vera, J., Granado, P. & McClay, K. Structural evolution of the Orange basin gravity-driven system, offshore Namibia. *Mar Pet Geol* **27**, 233–237 (2010).
11. Peel, E. J., Hossack, J. R. & Travis, C. J. Genetic structural provinces and salt tectonics of the Cenozoic offshore U.S. Gulf of Mexico: a preliminary analysis. In: *Salt Tectonics: A Global Perspective* (Eds Jackson, M. P. A., Roberts, D. G. & Snelson, S.). *AAPG Mem* **65**, 153–175 (1995).
12. Trudgill, B. D. *et al.* The Perdido Fold Belt, Northwestern Deep Gulf of Mexico. Part 1: Structural Geometry, Geolution and Regional Implications. *AAPG Bull* **83**, 88–113 (1999).
13. Ambrose, W. A. *et al.* Neogene tectonic, stratigraphic and play framework of the southern Laguna Madre-Tuxpan continental shelf, Gulf of Mexico. *AAPG Bull* **89**, 725–751 (2005).
14. Cobbold, P. R., Mourgues, R. & Boyd, K. Mechanism of thin-skinned detachment in the Amazon Fan: assessing the importance of fluid overpressure and hydrocarbon generation. *Mar Pet Geol* **21**, 1013–1025 (2004).
15. Canals, M. *et al.* Slope failure dynamics and impacts from seafloor and shallow sub-seafloor geophysical data: case studies from the COSTA project. *Mar Geol* **213**, 9–72, <https://doi.org/10.1016/j.margeo.2004.10.001> (2004).
16. Gee, M. J. R., Uy, H. S., Warren, J., Morley, C. K. & Lambiasi, J. J. The Brunei slide: a giant submarine landslide on the North West Borneo Margin revealed by 3D seismic data. *Mar Geol* **246**, 9–23, <https://doi.org/10.1016/j.margeo.2007.07.009> (2007).
17. Minelli, L. *et al.* Discovery of a gliding salt-detached megaslide, Calabria, Ionian Sea, Italy. *Geophys Res Lett* **40**, 4220–4224, <https://doi.org/10.1002/grl.50818> (2013).
18. Malinverno, A. & Ryan, W. B. F. Extension in the Tyrrhenian Sea and shortening in the Apennines as a result of arc migration driven by sinking of the lithosphere. *Tectonics* **5**, 227–245 (1986).
19. Faccenna, C., Becker, T. W., Pio Lucente, F., Jolivet, L. & Rossetti, F. History of subduction and back-arc extension in the Central Mediterranean. *Geophys J Int* **145**, 809–820 (2001).
20. Faccenna, C. *et al.* Constraints on mantle circulation around the deforming Calabrian slab. *Geophys Res Lett* **32**, L06311, <https://doi.org/10.1029/2004GL021874> (2005).
21. Sartori, R. The Tyrrhenian back-arc basin and subduction of the Ionian lithosphere. *Episodes* **26**, 217–221 (2003).
22. Guillaume, B., Funicello, F., Faccenna, C., Martinod, J. & Olivetti, V. Spreading pulses of the Tyrrhenian Sea during the narrowing of the Calabrian slab. *Geology* **38**, 819–822 (2010).
23. Van Dijk, J. P. Basin dynamics and sequence stratigraphy in the Calabrian Arc (Central Mediterranean): records and pathways of the Crotona Basin. *Geol Mijnb* **70**, 187–201 (1991).
24. Van Dijk, J. P. & Okkes, F. W. M. Neogene tectonostratigraphy and kinematics of Calabrian basins; implications for the geodynamics of the Central Mediterranean. *Tectonophysics* **196**, 23–60 (1991).
25. Van Dijk, J. P. *et al.* A regional structural model for the northern sector of the Calabrian Arc (southern Italy). *Tectonophysics* **324**, 267–320 (2000).
26. Roda, C. Distribuzione e facies dei sedimenti Neogenici nel Bacino Crotonese. *Geol Romana* **3**, 319–366 (1964).
27. Zecchin, M. *et al.* The Plio-Pleistocene evolution of the Crotona Basin (southern Italy): interplay between sedimentation, tectonics and eustasy in the frame of Calabrian Arc migration. *Earth Sci Rev* **115**, 273–303 (2012).
28. Zecchin, M. *et al.* The Messinian succession of the Crotona Basin (southern Italy) I: Stratigraphic architecture reconstructed by seismic and well data. *Mar Pet Geol* **48**, 455–473 (2013a).
29. Zecchin, M. *et al.* The Messinian succession of the Crotona Basin (southern Italy) II: Facies architecture and stratal surfaces across the Miocene-Pliocene boundary. *Mar Pet Geol* **48**, 474–492 (2013b).
30. Zecchin, M., Praeg, D., Ceramicola, S. & Muto, F. Onshore to offshore correlation of regional unconformities in the Plio-Pleistocene sedimentary successions of the Calabrian Arc (central Mediterranean). *Earth Sci Rev* **142**, 60–78, <https://doi.org/10.1016/j.earscirev.2015.01.006> (2015).
31. Massari, F. & Prosser, G. Late Cenozoic tectono-stratigraphic sequences of the Crotona Basin: insights on the geodynamic history of the Calabrian arc and Tyrrhenian Sea. *Basin Res* **25**, 26–51 (2013).
32. Zecchin, M., Caffau, M. & Ceramicola, S. Interplay between regional uplift and glacio-eustasy in the Crotona Basin (Calabria, southern Italy) since 0.45 Ma: a review. *Global Planet Change* **143**, 196–213 (2016).
33. Roveri, M., Bernasconi, A., Rossi, M. E. & Visentin, C. Sedimentary Evolution of the Luna Field Area, Calabria, Southern Italy. In: *Generation, Accumulation and Production of Europe's Hydrocarbons II*. (Ed. Spencer, A.M.). *Special Publication of the European Association of Petroleum Geoscientists* **2**, 217–224 (1992).
34. Capozzi, R. *et al.* Neogene to Quaternary tectonics and mud diapirism in the Gulf of Squillace (Crotona-Spartivento Basin, Calabrian Arc, Italy). *Mar Pet Geol* **35**, 219–234 (2012).
35. Zecchin, M., Massari, F., Mellere, D. & Prosser, G. Anatomy and evolution of a Mediterranean-type fault bounded basin: the Lower Pliocene of the northern Crotona Basin (Southern Italy). *Basin Res* **16**, 117–143 (2004).
36. Zecchin, M., Massari, F., Mellere, D. & Prosser, G. Architectural styles of prograding wedges in a tectonically active setting, Crotona Basin, Southern Italy. *J Geol Soc London* **160**, 863–880 (2003).
37. Consolaro, C., Macri, P., Massari, F., Speranza, F. & Fornaciari, E. A major change in the sedimentation regime in the Crotona Basin (Southern Italy) around 3.7–3.6 Ma. *Palaeogeogr Palaeoclimatol Palaeoecol* **392**, 398–410 (2013).
38. Muto, F. *et al.* A Neogene-Quaternary Geotraverse within the northern Calabrian Arc from the foreland peri-Ionian margin to the backarc Tyrrhenian margin. *Geol. Field Trips* **7(2.2)**, 1–65, <https://doi.org/10.3301/GFT.2015.04> (2015).
39. Choen, J. W. & Stockwell, J. W., Jr. CWP/SU: Seismic Un\*x Release No. 44: an open source software package for seismic research and processing (2016).
40. Costantini, M. *et al.* Analysis of surface deformations over the whole Italian territory by interferometric processing of ERS, Envisat and COSMO-SkyMed radar data. *Rem Sens Environ* <https://doi.org/10.1016/j.rse.2017.07.017> (2017).
41. Teatini, P. *et al.* Resolving land subsidence within the Venice Lagoon by persistent scatterer SAR interferometry. *Phys Chem of the Earth, Parts A/B/C* **40-41**, 72–79, <https://doi.org/10.1016/j.pce.2010.01.002> (2012).
42. Tosi, L., Strozzi, T., Da Lio, C. & Teatini, P. Regional and local land subsidence at the Venice coastland by TerraSAR-X PSI. *Proc IAHS* **372**, 199–205, <https://doi.org/10.5194/piahs-372-199-2015> (2015).

43. Da Lio C., Teatini P., Strozzi T. & Tosi L. Understanding land subsidence in salt marshes of the Venice lagoon from SAR Interferometry and ground-based investigations. *Rem Sens Environ*, <https://doi.org/10.1016/j.rse.2017.11.016> (2018).
44. Teatini, P. *et al.* Geomechanical response to seasonal gas storage in depleted reservoirs: A case study in the Po River basin, Italy. *J Geophys Res* **116**, F02002, <https://doi.org/10.1029/2010JF001793> (2011).
45. Tamburini, A., Bianchi, M., Giannico, C. & Novali, F. Retrieving surface deformation by PSInSAR technology: A powerful tool in reservoir monitoring. *Int J Greenhouse Gas Control* **4**, 928–937, <https://doi.org/10.1016/j.ijggc.2009.12.009> (2010).

## Acknowledgements

Data used in this study were acquired in the framework of several national projects: MaGIC (Marine Geohazards along the Italian Coasts), funded by the Italian Civil Protection Department, CARG (Cartografia Geologica Italiana), funded by Istituto Superiore per la Protezione e la Ricerca Ambientale (ISPRA), and RITMARE - The Italian Research for the Sea - coordinated by the Italian National Research Council and funded by the Italian Ministry of Education, University and Research within the National Research Program 2011–2013. Data courtesy: ViDEPI Project (<http://unmig.sviluppoeconomico.gov.it/videpi/>); COSMO-SkyMed Persistent Scatterer Interferometry products made available by the Italian Ministry of the Environment and Protection of Land and Sea; GPS time series, Nevada Geodetic Laboratory (NGL), available from <http://geodesy.unr.edu/>; public DTM data available from <https://www2.jpl.nasa.gov/srmt/>. We thank two anonymous reviewers for helpful and constructive comments during the review process.

## Author Contributions

M.Z., S.Ce., D.C., C.D.L., G.M., G.P., P.T. and L.T. interpreted data; M.Z. wrote the initial manuscript draft and prepared the figures; F.A. processed the seismic lines; S.Ce. acquired and interpreted swath bathymetry and subbottom data; C.D.L., P.T. and L.T. worked on GPS and interferometric data; all authors discussed and commented on the methods and results and contributed to the paper's final version.

## Additional Information

**Supplementary information** accompanies this paper at <https://doi.org/10.1038/s41598-018-26266-y>.

**Competing Interests:** The authors declare no competing interests.

**Publisher's note:** Springer Nature remains neutral with regard to jurisdictional claims in published maps and institutional affiliations.



**Open Access** This article is licensed under a Creative Commons Attribution 4.0 International License, which permits use, sharing, adaptation, distribution and reproduction in any medium or format, as long as you give appropriate credit to the original author(s) and the source, provide a link to the Creative Commons license, and indicate if changes were made. The images or other third party material in this article are included in the article's Creative Commons license, unless indicated otherwise in a credit line to the material. If material is not included in the article's Creative Commons license and your intended use is not permitted by statutory regulation or exceeds the permitted use, you will need to obtain permission directly from the copyright holder. To view a copy of this license, visit <http://creativecommons.org/licenses/by/4.0/>.

© The Author(s) 2018